Robust Sensorless Control Against Thermally Degraded Speed Performance in an IM Drive Based Electric Vehicle

S. M. Nawazish Ali, *Member, IEEE,* M. J. Hossain, *Senior Member, IEEE,* Dong Wang, *Member, IEEE,* Kaiyuan Lu, *Member, IEEE,* Peter Omand Rasmussen, *Member, IEEE,* Vivek Sharma, *Member, IEEE,* Muhammad Kashif, *Member, IEEE*

***Abstract*—This paper investigates and proposes an efficient control design to address the degradation in the mechanical speed of a traction machine drive (TMD) in an electric vehicle (EV) caused by thermal effects during its operation. Variations in the operating as well as ambient temperature cause unexpected uncertainties in TMD parameters such as stator and rotor resistance, which results in significant degradation in EV's speed performance capability. To mitigate this problem, an output feedback robust linear parameter varying (LPV) controller-observer set is designed using $\mathbf{H}_\infty$ control theory that enhances the EV's speed performance in field-oriented control (FOC) frame. The internal stability of the closed-loop control and the L_2 gain bound are ensured by linear matrix inequalities. The performance of the proposed control technique is compared with that of conventional FOC, sliding mode control (SMC) and higher order sliding mode control (HOSMC) to validate its efficacy and advantages. The robustness of the proposed control technique is tested for an EV operation against the Worldwide Harmonised Light Vehicles Test Procedure (WLTP) Class 3 driving cycle. The nonlinear MATLAB simulation results guarantee the effectiveness of the proposed controller-observer set. These results are verified experimentally on an induction machine drive setup.**

***Index Terms*—Induction machine drive, Degraded speed performance, Sensorless linear parameter varying (LPV) control, Electric vehicle**

I. Introduction

Global warming, limited reserves, vastly fluctuating prices and emissions of greenhouse gas are the major hitches regarding fossil fuels, where transportation sector is its major consumer. This inevitable consumption of fossil fuels can be reduced by the electrification of vehicles, which results in the production of zero emission and eco-friendly electric vehicles [1].

The most significant component in an EV is the traction machine drive (TMD) of its propulsion system which is solely responsible for converting the battery electrical energy into the vehicle mechanical energy in the form of traction force with appropriate torque and speed [2]. In terms of its control design, a TMD is dominant over internal combustion engine due to its individual wheel control and fast electromagnetic torque response [3]. Among the available traction machines, the induction machine (IM) shows a promising performance in the automotive sector (EV/HEV) such as in the Honda Fit EV (2012), Chevrolet (USA), Tesla Model (2012), Toyota RAV4 EV (2012), BMW/X5 (Germany), Renault/Kangoo (1998) and Durango (USA) [4]. This is mainly because of its wide speed operation, higher power density, greater starting torque, less maintenance and de-excitation for inverter fault [5].

Traditional control techniques such as FOC are preferred for efficient performance of IM drive based EV, but its operation suffers from parameter variations (stator and rotor resistance) resulting in thermal degradation of the electrified powertrain performance [6]. This variation is caused by capricious EV operating conditions, mainly due to driving cycle schedules, traffic state, temperature and vehicle loading [7]. This problem poses the necessity of implementing a robust closed-loop control technique to enhance the dynamic performance of the EV.

Sensorless speed control through rotor flux estimation is the core requirement for mitigating the effect of parameter variation resulting in conventional FOC deterioration. It gives a maintenance free and reliable IM drive operation [8]. Thermal degradation of rotor flux has a key role in FOC deterioration, causing a significant decrease in performance efficiency and an increase in drive energy consumption [9]. For speed estimation using sensorless conventional FOC, various methods such as slip calculation are used. It requires the estimation of stator field and slip speed. Rotor or mechanical speed is obtained by their difference. Since the estimated slip speed is proportional to the rotor resistance, the actual slip speed increases by the increase in temperature which results in significant degradation in rotor speed of IM caused by thermal effects. This problem can only be addressed by estimating the rotor speed more accurately even in the presence of varying rotor resistance using a robust observer.

Some of the IM flux estimation techniques for EV/HEV application in the literature are Luenberger Observer, Extended Kalman filter [10], and rotor flux adaptive observer [11]. Sliding mode control (SMC) is also used in the literature for IM based EV/HEV speed control estimation [12]–[14]. Although robust, the SMC technique has chattering issues that makes it difficult to get the desired speed and optimal

Dong Wang, Kaiyuan Lu and Peter Omand Rasmussen are with the Department of Energy Technology, Aalborg University, DK-9220 Aalborg, Denmark. (e-mail: dwa@et.aau.dk; klu@et.aau.dk; por@et.aau.dk).

S. M. Nawazish Ali, M. J. Hossain, Vivek Sharma and Muhammad Kashif are with the School of Engineering, Macquarie University, Sydney, NSW, 2109 Australia. (e-mail: syed-muhammad-nawazish.ali@hdr.mq.edu.au; jahangir.hossain@mq.edu.au; vivek.sharma2@hdr.mq.edu.au; muhammad.kashif@hdr.mq.edu.au).

flux for EV/HEV application. In view of this problem, higher order sliding mode (HOSM) control is addressed in [15]–[17] for IM, but these works are not in the context of EV/HEV application. In comparison with a fixed observer, that ignores the plant's dynamic nature, a linear parameter varying (LPV) observer can give better performance and robustness [18].

An LPV observer design has been presented in [19] for IM but its implementation only considers the load torque and the rotor resistance variations. An LPV based robust observer has been given in [20] but it considers only 20% rotor resistance variation, and stator resistance variation is neglected. Similarly, only variations in the rotor resistance have been incorporated in the LPV design in [21]. The LPV observer design for IM given in [19]–[21] is purely for industrial applications and comes with excess computational time. But in EV applications, speed and temperature variations are quite significant. As a result, a robust LPV observer is proposed in this research that considers both the stator and rotor resistance and also addresses the estimation of speed degradation for efficient EV operation.

The linear parameter varying (LPV) control technique has been addressed for IM drive control by many researchers. It gives more robustness and gain scheduling without changing the actual plant dynamics [22]. An IM control scheme has been given in [23] using quasi LPV control. An LPV control scheme for IM shaft angle and mechanical speed has been discussed in [24], although resistance variations are not addressed. An LPV control scheme has been developed in [25] for IM speed, rotor resistance and rotor current frequency but it ignores the effect of varying stator resistance.

Authors have recently reported thermally deteriorated dynamic response for an LPV controlled IM in [26]. The mentioned existing LPV-IM control studies are not in the context of EV/HEV applications and only presented preliminary results. As per the author's knowledge, the LPV control technique has not been implemented in the literature to cater for the thermally degraded speed of an EV due to varying surrounding and operating temperatures. There is a definite need to design and implement such a robust control technique that gives excellent tracking performance against a standard EV driving cycle for a flexible range of parameter variations. The major contribution of this work is the design and implementation of an LPV based controller-observer set to address the thermally degraded speed of the traction motor (IM) drive of an EV and its analysis under a standard driving cycle.

The proposed control and estimation of the LPV scheme enhances the EV speed performance and is tested against a WLTP Class 3 as per the evaluation standard by the automotive community [27]. Simulation results are validated through comparison with counter control techniques and also by an experimental setup of an IM drive. The remaining paper is organized as follows: Section II presents IM, EV and LPV mathematical modeling. Section III elaborates the performance analysis of EV and IM. Section IV provides thermally degraded speed estimation through a robust LPV observer. Section V discusses the LPV control architecture and design. Section VI gives the comparison of LPV based FOC with conventional and HOSMC based FOC. Section VII presents the performance validation of the overall EV control system against NEDC through MATLAB-based simulations. Section VIII presents the experimental validation of the simulation results using an IM electrical drive setup. Section IX gives conclusion and proposed future work.

TABLE I: IM Parameters

Parameter	Value
number of pole-pairs (n_P)	2
magnetizing inductance (L_m)	0.04 H
stator self-inductance (L_s)	0.0425 H
stator resistance (R_s)	0.22 Ω
rotor self-inductance (L_r)	0.043 H
rotor resistance (R_r)	0.209 Ω
damping coefficient (B)	0.01 N.m.sec.rad^{-1}
moment of inertia (J)	0.124 kg.m^2

II. IM AND EV MODELLING

A. IM Nonlinear Modelling

An $\alpha-\beta$ axis IM mathematical model in stationary reference frame is given as [26]:

$$\begin{bmatrix}\dot{i}_{\alpha s}\\ \dot{i}_{\beta s}\\ \dot{\psi}_{\alpha r}\\ \dot{\psi}_{\beta r}\end{bmatrix} = \begin{bmatrix}\mathbf{A_{11}} & \mathbf{A_{12}}\\ \mathbf{A_{21}} & \mathbf{A_{22}}\end{bmatrix}\begin{bmatrix}i_{\alpha s}\\ i_{\beta s}\\ \psi_{\alpha r}\\ \psi_{\beta r}\end{bmatrix} + \begin{bmatrix}\mathbf{U_1}\\ \mathbf{U_2}\end{bmatrix}\mathbf{V_s} \tag{1}$$

$$\begin{bmatrix}\dot{i}_{\alpha s}\\ \dot{i}_{\beta s}\\ \dot{\psi}_{\alpha r}\\ \dot{\psi}_{\beta r}\end{bmatrix} = \begin{bmatrix}-a_{11} & 0 & a_{12} & n_P a_{12}\omega_r\\ 0 & -a_{11} & -n_P a_{12}\omega_r & a_{12}\\ R_r a_{21} & 0 & -a_{22} & -n_P\omega_r\\ 0 & R_r a_{21} & n_P\omega_r & -a_{22}\end{bmatrix}\begin{bmatrix}i_{\alpha s}\\ i_{\beta s}\\ \psi_{\alpha r}\\ \psi_{\beta r}\end{bmatrix} + \begin{bmatrix}u_1 & 0\\ 0 & u_1\\ u_2 & u_2\\ u_2 & u_2\end{bmatrix}\begin{bmatrix}V_{\alpha s}\\ V_{\beta s}\end{bmatrix} \tag{2}$$

where $a_{11} = \frac{(L_m^2 R_r + L_r^2 R_s)}{\sigma L_s L_r^2}$, $a_{12} = \frac{L_m R_r}{\sigma L_s L_r^2}$, $a_{21} = \frac{L_m}{L_r}$, $a_{22} = \frac{R_r}{L_r}$, $u_1 = \frac{1}{\sigma L_s}$, $u_2 = 0$, $\sigma = 1 - (\frac{L_m}{L_s})a_{21}$. The IM parameters and their rated values are given in Table I. The IM generated rotor flux, electromagnetic torque and mechanical speed are given as follows:

$$\psi_r = \sqrt{\psi_{\alpha r}^2 + \psi_{\beta r}^2} \tag{3}$$

$$\tau_E = (3/2)n_P a_{21}(\psi_{\alpha r} i_{\beta s} - \psi_{\beta r} i_{\alpha s}) \tag{4}$$

$$\omega_r = \int \frac{3}{2}\frac{n_P L_m}{J L_r}(\psi_{\alpha r} i_{\beta s} - \psi_{\beta r} i_{\alpha s}) - (\frac{B}{J}\omega_r) - (\frac{1}{J}\tau_L) \tag{5}$$

where $i_{\alpha s}$, $i_{\beta s}$, $\psi_{\alpha r}$, $\psi_{\beta r}$ and τ_L are the $\alpha-\beta$ axis stator currents, rotor fluxes and load torque respectively.

B. EV Dynamics

The varying resistance's effect on IM is further extended to the dynamics of an electric vehicle. The EV model's aerodynamics and mechanics principles are given in [10]. The wheel drive regarding motor referential is described by the following vehicle speed expression:

$$\dot{\omega}_r = n_P(\frac{\tau_E}{J} - \frac{\tau_{L(EV)}}{J} - \frac{B\omega_r}{J}) \tag{6}$$

The EV traction force is given as:

$$F_{trac} = F_{in} + F_{ae} + F_{gr} + F_{ro} \tag{7}$$

where F_{in} is the inertial resistance force, F_{ae} is the aerodynamic drag force, F_{ro} is the rolling resistance force and F_{gr} is the grade force. The EV power for compensating F_{trac} at a vehicle speed n_R is given by:

$$P_{EV} = n_R F_{trac} \tag{8}$$

$$n_R = \frac{R_{tire}}{G_r}\omega_r \tag{9}$$

The EV load torque is given as:

$$\tau_{L(EV)} = \frac{F_{trac} R_{tire}}{G_r} \tag{10}$$

where R_{tire} is the tire radius and G_r is the gear ratio.

C. LPV Modeling

The nonlinear IM model is converted into an LPV model which is as follows:

$$\mathbf{G}(\mathbf{\Theta(t)}) : \frac{\mathbf{d}}{\mathbf{dt}}\mathbf{x} = \mathbf{A}(\mathbf{\Theta(t)})\mathbf{x} + \mathbf{B}(\mathbf{\Theta(t)})\mathbf{u}$$
$$\mathbf{y} = \mathbf{C}(\mathbf{\Theta(t)})\mathbf{x} + \mathbf{D}(\mathbf{\Theta(t)})\mathbf{u} \tag{11}$$

where $\mathbf{\Theta(t)}=[\Theta_1\ \Theta_2]^T=[R_s(t)\ R_r(t)]^T$ is a parameter varying with respect to time. The LPV system matrix is given as:

$$\mathbf{A}(\mathbf{\Theta(t)}) = \begin{bmatrix} -(\frac{\Theta_1}{\xi} + \frac{\Theta_2 a_{21}^2}{\xi}) & 0 & \frac{a_{21}\Theta_2}{\xi L_r} & \frac{n_P \omega_r a_{21}}{\xi} \\ 0 & -(\frac{\Theta_1}{\xi} + \frac{\Theta_2 a_{21}^2}{\xi}) & -\frac{n_P \omega_r a_{21}}{\xi} & \frac{a_{21}\Theta_2}{\xi L_r} \\ a_{21}\Theta_2 & 0 & -\frac{\Theta_2}{L_r} & -n_P\omega_r \\ 0 & a_{21}\Theta_2 & n_P\omega_r & -\frac{\Theta_2}{L_r} \end{bmatrix}$$

$$\mathbf{B} = \begin{bmatrix} \frac{1}{\xi} & 0 \\ 0 & \frac{1}{\xi} \\ 0 & 0 \\ 0 & 0 \end{bmatrix}, \mathbf{C} = \begin{bmatrix} 1 & 0 & 0 & 0 \\ 0 & 1 & 0 & 0 \end{bmatrix}, \mathbf{D} = \begin{bmatrix} 0 & 0 \\ 0 & 0 \end{bmatrix} \tag{12}$$

where $\xi = \sigma L_s$. **B**, **C**, **D** are fixed matrices. The input, state and output vectors are given by:

$$\mathbf{u(t)} = [V_{\alpha s}\ V_{\beta s}]^T, \mathbf{x(t)} = [i_{\alpha s}\ i_{\beta s}\ \psi_{\alpha r}\ \psi_{\beta r}]^T, \mathbf{y(t)} = [i_{\alpha s}\ i_{\beta s}]^T \tag{13}$$

III. EV and IM Performance Analysis

A. Performance Constraints

The performance of an electric vehicle depends significantly upon its terminal characteristics, mainly mechanical speed. Variations in the operating as well as the ambient temperature cause thermal degradation in the speed of the TMD of an EV that ultimately reduce its propulsion tendency and performance efficiency.

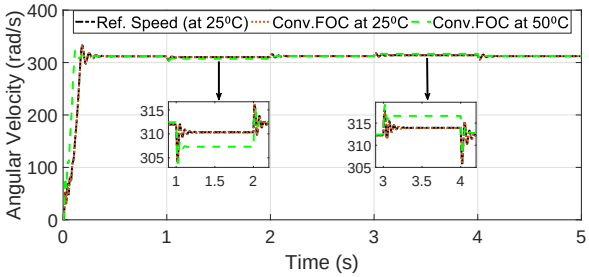

Fig. 1: Thermally degraded speed of IM with sensorless conventional FOC

B. Thermally Degraded Speed of IM with conventional FOC

The mechanical speed of IM with sensorless conventional FOC is evaluated against varying temperatures and shows vivid thermal degradation as given in Fig. 1. The values of the machine parameters (resistances) used in both machine model and controller are the values at 25°C. It can be observed from Fig. 1 that at 25°C machine temperature, the machine speed can be kept equal to the reference speed profile (obtained from [28]) by using conventional FOC. However, when the machine temperature increases to 50°C which can be caused by vehicle loading, traffic state etc. in EV operating conditions, the machine's stator and rotor resistance will increase. Then, the machine speed cannot be maintained at its reference speed as the values of stator and rotor resistance used in the controller are still the same as at 25°C. It can be seen in the zoomed plots, the speed drops to 307.4 rad/s during 1∼2s when full load is applied to IM in motor mode, and the speed increases to 316.5 rad/s during 3∼4s when full load is applied to IM in generator mode. This is due to the reason that the slip speed estimation in the controller is based on the rotor resistance at 25°C, while the actual rotor resistance at 50°C is higher. Thus, the slip speed is under-estimated, which results in under-compensation of rotor speed in motor mode or over-compensation in generator mode. When the IM temperature increases from ambient to the maximum operating temperature, there occurs a 20-50% change in its resistances. In the case of high power IM, the operating temperature exceeds to a maximum value of 140°C [29], which leads to a significant speed degradation issue with the performance of conventional FOC at higher temperatures. This gives the motivation to design an LPV controller-observer set to address this speed degradation issue due to thermal effects as well as to estimate the mechanical speed more accurately in the presence of varying parameters.

IV. Thermally Degraded Speed Estimation by LPV Observer

The performance of IM drive in the propulsion system of an EV primarily depends on the FOC method, which relies significantly on an accurate rotor flux estimation. However, variations in the IM electrical parameters make it less precise. Temperature variations result in change in the stator as well as the rotor resistance that cause inaccuracy in the estimation of rotor flux. This behavior is due to its dependence on the

resistance temperature coefficient of the material given by [30]:

$$R = R_0[1 + \alpha \Delta T] \tag{14}$$

where α is the resistance temperature coefficient, R_0 is the conductor resistance at the reference temperature and ΔT is the temperature difference. Hence, the drive speed performance is degraded due to the imprecise rotor flux estimation. In order to monitor the EV drive performance, it is necessary to estimate the thermally degraded speed so that it can be enhanced as per the desired control objectives. Hence, an LPV robust observer is developed to cater for the thermal degradation due to resistance variations during vehicle operation. The structure of the LPV observer is given by:

$$\begin{bmatrix} \dot{\hat{\mathbf{i}}}^{\mathbf{s}}_{\mathbf{S}} \\ \dot{\hat{\boldsymbol{\psi}}}^{\mathbf{s}}_{\mathbf{r}} \end{bmatrix} = \begin{bmatrix} \mathbf{A_{11}}(\boldsymbol{\Theta}) & \mathbf{A_{12}}(\boldsymbol{\Theta}) \\ \mathbf{A_{21}}(\boldsymbol{\Theta}) & \mathbf{A_{22}}(\boldsymbol{\Theta}) \end{bmatrix} \begin{bmatrix} \hat{\mathbf{i}}^{\mathbf{s}}_{\mathbf{S}} \\ \hat{\boldsymbol{\psi}}^{\mathbf{s}}_{\mathbf{r}} \end{bmatrix} + \mathbf{B}\mathbf{V}^{\mathbf{s}}_{\mathbf{S}} + \mathbf{L}(\boldsymbol{\Theta}) \left\{ \mathbf{i}^{\mathbf{s}}_{\mathbf{S}} - \mathbf{C} \begin{bmatrix} \hat{\mathbf{i}}^{\mathbf{s}}_{\mathbf{S}} \\ \hat{\boldsymbol{\psi}}^{\mathbf{s}}_{\mathbf{r}} \end{bmatrix} \right\} \tag{15}$$

where $\mathbf{i^s_S} = [i_{\alpha s}\ i_{\beta s}]^T$, $\boldsymbol{\psi}^{\mathbf{s}}_{\mathbf{r}} = [\psi_{\alpha r}\ \psi_{\beta r}]^T$, $\mathbf{V^s_S} = [V_{\alpha s}\ V_{\beta s}]^T$ and $\mathbf{L}(\boldsymbol{\Theta})$ is the observer gain matrix. The error equation in the observer design can be extracted from the stator currents and rotor fluxes as follows:

$$\mathbf{e} = \begin{bmatrix} \mathbf{i}^{\mathbf{s}}_{\mathbf{S}} \\ \boldsymbol{\psi}^{\mathbf{s}}_{\mathbf{r}} \end{bmatrix} - \begin{bmatrix} \hat{\mathbf{i}}^{\mathbf{s}}_{\mathbf{S}} \\ \hat{\boldsymbol{\psi}}^{\mathbf{s}}_{\mathbf{r}} \end{bmatrix} \tag{16}$$

The observer gain matrix $\mathbf{L}(\boldsymbol{\Theta})$ can be computed from state space form of (16) which is given as:

$$\dot{\mathbf{e}} = \left(\begin{bmatrix} \mathbf{A_{11}}(\boldsymbol{\Theta}) & \mathbf{A_{12}}(\boldsymbol{\Theta}) \\ \mathbf{A_{21}}(\boldsymbol{\Theta}) & \mathbf{A_{22}}(\boldsymbol{\Theta}) \end{bmatrix} - \mathbf{L}(\boldsymbol{\Theta})\mathbf{C} \right) \mathbf{e} \tag{17}$$

The estimated mechanical speed is given by:

$$\hat{\omega}_r = \int \frac{3}{2} \frac{n_P L_m}{J L_r} (\hat{\psi}_{\alpha r} i_{\beta s} - \hat{\psi}_{\beta r} i_{\alpha s}) - (\frac{B}{J} \hat{\omega}_r) - (\frac{1}{J} \tau_L) \tag{18}$$

V. LPV Control Architecture

The overall LPV control of IM based architecture is presented in Fig. 2. It comprises three types of controller blocks. The LPV controller blocks act as current controllers scheduled with varying machine resistances of the LPV model of an IM given in (12) and track the stator currents of an IM. On the other hand, speed and flux controllers are based on an input-output feedback linearization technique as explained in Section V-C and generates the stator reference currents through a regulator of appropriate gain values from the speed and flux obtained from the robust LPV observer. All these controllers collectively ensure the correct IM flux and speed tracking.

A. LPV Current Controller

The design constraints and specifications in LPV control framework are expressed in terms of generalized plant. Its state space representation in matrix form is given by:

$$\begin{bmatrix} \dot{\mathbf{x}} \\ \mathbf{z} \\ \mathbf{y} \end{bmatrix} = \begin{bmatrix} \mathbf{A}(\boldsymbol{\Theta}) & \mathbf{B_w}(\boldsymbol{\Theta}) & \mathbf{B_u}(\boldsymbol{\Theta}) \\ \mathbf{C_z}(\boldsymbol{\Theta}) & \mathbf{D_{zw}}(\boldsymbol{\Theta}) & \mathbf{D_{zu}}(\boldsymbol{\Theta}) \\ \mathbf{C_y}(\boldsymbol{\Theta}) & \mathbf{D_{yw}}(\boldsymbol{\Theta}) & \mathbf{0} \end{bmatrix} \begin{bmatrix} \mathbf{x} \\ \mathbf{w} \\ \mathbf{u} \end{bmatrix} \tag{19}$$

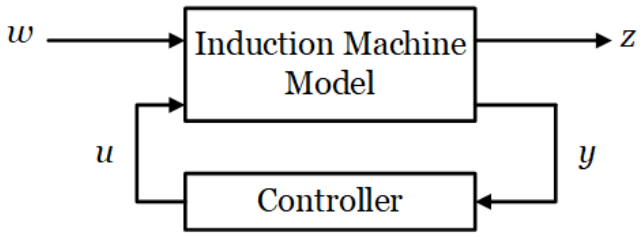

Fig. 3: LPV generalized plant structure

where $\mathbf{z}$ is the controlled output vector explained in Section V-B and $\mathbf{w} = [i_{\alpha sref}\ \ i_{\beta sref}]^T$ is the external input vector. An LPV generalized plant structure is given in Fig. 3. $\mathbf{A}$, $\mathbf{B_w}$, $\mathbf{B_u}$, $\mathbf{C_z}$, $\mathbf{D_{zw}}$, $\mathbf{D_{zu}}$, $\mathbf{C_y}$ and $\mathbf{D_{yw}}$ are the system matrices. Θ is the time varying parameter that can be represented as:

$$\boldsymbol{\Theta}(\mathbf{t}) = (\Theta_1, \Theta_2, ..., \Theta_N)^T \tag{20}$$

The range of each Θ_i is given by:

$$\Theta_i(t)\ \epsilon\ [\Theta_{min}\ \Theta_{max}] \tag{21}$$

The matrix $\mathbf{A}(\boldsymbol{\Theta}(\mathbf{t}))$ can be expanded as:

$$\begin{aligned} \mathbf{A}\left(\boldsymbol{\Theta}(\mathbf{t})\right) &= \mathbf{A}\left(R_s, R_r\right) = \mathbf{A_0} + \Theta_1 \mathbf{A_1} + \Theta_2 \mathbf{A_2} \\ \mathbf{A}\left(\boldsymbol{\Theta}(\mathbf{t})\right) &= \mathbf{A_0} + R_s \mathbf{A_1} + R_r \mathbf{A_2} \end{aligned} \tag{22}$$

The convex decomposition for $\boldsymbol{\Theta}(\mathbf{t})$ is:

$$\boldsymbol{\Theta}(\mathbf{t}) = \alpha_1 \Theta_{11} + \alpha_2 \Theta_{12} + \alpha_3 \Theta_{21} + \alpha_4 \Theta_{22} \tag{23}$$

with

$$\sum_{i=1}^{4} \alpha_i = 1\ and\ \alpha_i \geq 0$$

where α_i is the corner for the polytopic parameter range. Corner values for the polytopic parameter range are:

$$\begin{aligned} \Theta_{11} &= (0, R_{smin}), \Theta_{12} = (0, R_{smax}) \\ \Theta_{21} &= (0, R_{rmin}), \Theta_{22} = (0, R_{rmax}) \end{aligned} \tag{24}$$

The IM polytopic plant model for vertex values of Θ is as follows:

$$\mathbf{G}(\boldsymbol{\Theta}) = \alpha_1 \mathbf{G}(\Theta_{11}) + \alpha_2 \mathbf{G}(\Theta_{12}) + \alpha_3 \mathbf{G}(\Theta_{21}) + \alpha_4 \mathbf{G}(\Theta_{22}) \tag{25}$$

$$\begin{aligned} \alpha_1 &= \frac{R_s(t) - R_{s\,min}}{R_{s\,max} - R_{s\,min}}, \alpha_2 = \frac{R_s(t) - R_{s\,max}}{R_{s\,max} - R_{s\,min}} \\ \alpha_3 &= \frac{R_r(t) - R_{r\,min}}{R_{r\,max} - R_{r\,min}}, \alpha_4 = \frac{R_r(t) - R_{r\,max}}{R_{r\,max} - R_{r\,min}} \end{aligned} \tag{26}$$

The state space representation of LPV output feedback controller dynamics in matrix form is given by:

$$\begin{bmatrix} \dot{\mathbf{x_K}} \\ \mathbf{u} \end{bmatrix} = \begin{bmatrix} \mathbf{A_K}(\boldsymbol{\Theta}) & \mathbf{B_K}(\boldsymbol{\Theta}) \\ \mathbf{C_K}(\boldsymbol{\Theta}) & \mathbf{D_K}(\boldsymbol{\Theta}) \end{bmatrix} \begin{bmatrix} \mathbf{x_K} \\ \mathbf{y} \end{bmatrix} \tag{27}$$

such that it ensures internal stability and induced L_2 norm of the closed-loop control system (formed by (19) and (27)) bounded by $\gamma > 0$ from external input $\mathbf{w}$ to control output $\mathbf{z}$ i.e.,

$$\frac{\int_0^L \mathbf{z}^T(t)\mathbf{z}(t)dL}{\int_L^0 \mathbf{w}^T(t)\mathbf{w}(t)dL} \leq \gamma^2, \forall \mathbf{w}(t) \neq 0, L \geq 0$$

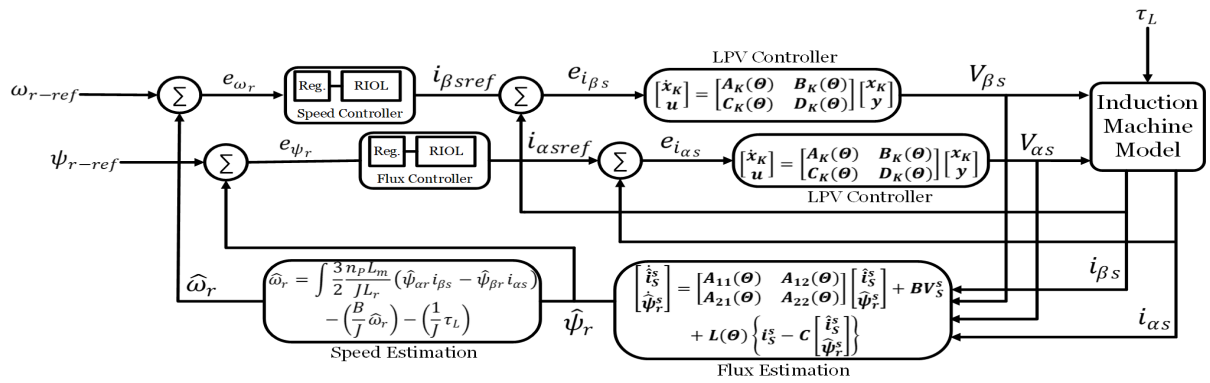

Fig. 2: LPV based induction machine control architecture

where $\mathbf{A_K}$, $\mathbf{B_K}$, $\mathbf{C_K}$ and $\mathbf{D_K}$ are the controller matrices that can be calculated as (28). The gain matrices $\mathbf{A_K}(\Theta_i)$, $\mathbf{B_K}(\Theta_i)$, $\mathbf{C_K}(\Theta_i)$ and $\mathbf{D_K}(\Theta_i)$ can be obtained according to the following Theorem 1. There are six states of LPV controller out of which two originate from $\mathbf{W_s}$ as explained in Section V-B and four states come from IM model.

Theorem 1. *For the LPV polytopic system (eq. (19)), consider the constrained trajectories of the frozen parameter $\Theta(t)$ (eq. (21)). There exists an LPV gain scheduling output feedback controller (eq. (27)) that enforces $\gamma > 0$ (upper bound) and overall closed loop stability on the induced L_2-norm of the closed-loop control system only if there exists $\boldsymbol{N}(\boldsymbol{\Theta})$ and $\boldsymbol{M}(\boldsymbol{\Theta})$ (symmetric parameter dependent matrices) and gain matrices $\widetilde{\boldsymbol{A}}_{\boldsymbol{K}}(\boldsymbol{\Theta})$, $\widetilde{\boldsymbol{B}}_{\boldsymbol{K}}(\boldsymbol{\Theta})$, $\widetilde{\boldsymbol{C}}_{\boldsymbol{K}}(\boldsymbol{\Theta})$ and $\widetilde{\boldsymbol{D}}_{\boldsymbol{K}}(\boldsymbol{\Theta})$ such that [26].*

Proof. See [31]. The obtainment of $\mathbf{A_K}(\Theta_i)$, $\mathbf{B_K}(\Theta_i)$, $\mathbf{C_K}(\Theta_i)$ and $\mathbf{D_K}(\Theta_i)$ from $\mathbf{N}(\boldsymbol{\Theta})$, $\mathbf{M}(\boldsymbol{\Theta})$, $\widetilde{\mathbf{A}}_{\mathbf{K}}(\boldsymbol{\Theta})$, $\widetilde{\mathbf{B}}_{\mathbf{K}}(\boldsymbol{\Theta})$, $\widetilde{\mathbf{C}}_{\mathbf{K}}(\boldsymbol{\Theta})$ and $\widetilde{\mathbf{D}}_{\mathbf{K}}(\boldsymbol{\Theta})$ can be found in [26], [31]. The polytopic LPV controller structure after simplification is given by:

$$\begin{bmatrix} \mathbf{A_K}(\boldsymbol{\Theta}) & \mathbf{B_K}(\boldsymbol{\Theta}) \\ \mathbf{C_K}(\boldsymbol{\Theta}) & \mathbf{D_K}(\boldsymbol{\Theta}) \end{bmatrix} = \sum_{i=1}^{4} \alpha_i \begin{bmatrix} \mathbf{A_K}(\boldsymbol{\Theta}_i) & \mathbf{B_K}(\boldsymbol{\Theta}_i) \\ \mathbf{C_K}(\boldsymbol{\Theta}_i) & \mathbf{D_K}(\boldsymbol{\Theta}_i) \end{bmatrix} \tag{28}$$

B. H_∞ Theory Based Design Objectives

In LPV framework, H_∞ norm of the closed-loop system is an alternate to the L_2 gain [22]. The proposed LPV controller for an IM is designed using H_∞ sensitivity gains. The design objectives are to:

1. ensure IM (plant) stability under varying parameters
2. provide an excellent tracking even in the presence of disturbances like load torque
3. develop an ability to reject noise and to handle the actuator constraints

A mixed H_∞ sensitivity gain structure for loop shaping is used to achieve these design objectives. The weighting gains obtained after tuning are used in control design as given in Table II [26]. Here, $\mathbf{w}$ given in (19) illustrates the reference input $\mathbf{r} = [i_{\alpha s} \;\; i_{\beta s}]^T$ in [26]. On the other hand, the vector $\mathbf{z}$ in (19) is $[z_1 \;\; z_2 \;\; z_3]^T = [z_s \;\; z_t \;\; z_{ks}]^T$. It comprises the output of weighting gain matrices $\mathbf{W_s}$, $\mathbf{W_t}$ and $\mathbf{W_{ks}}$. They are responsible for loop shaping of sensitivities. LPV controller gains are calculated by solving the linear matrix inequalities in [26] with the weighting gain functions. The optimal achieved value of γ is 0.8020.

TABLE II: H_∞ Weighting Gains

Weighting Gain	Value
Control sensitivity ($\mathbf{W_{ks}}$)	1/200
Sensitivity ($\mathbf{W_s}$)	$\frac{(1/M_s)s+w_B}{s+w_B A}$ A=factor for attenuation=1/500 M_s=sensitivity upper bound=2.0 w_B=bandwidth=550
Complementary sensitivity ($\mathbf{W_t}$)	$\frac{(0)s+w_T}{(0)s+1}$ w_T=0.8

C. Robust Speed and Flux Controller

The tracking of speed and flux is achieved by a robust input-output feedback linearization (RIOL) approach [26]. The input and output vectors are $\mathbf{i_S^s} = [i_{\alpha s} \;\; i_{\beta s}]^T$ and $\mathbf{y} = [\omega_r \;\; \psi_r]^T$ respectively. By differentiating the flux and speed relations, the $\alpha - \beta$ axis stator reference currents are generated through a regulator (labelled as Reg. in Fig. 2) of appropriate gain values. The reference currents are given as follows:

$$i_{\alpha sref} = \frac{\hat{\psi}_{\alpha r}}{\lambda_3}\left(\frac{\dot{\hat{\psi}}_r}{\hat{\psi}_r} + \lambda_2\right) + \frac{\hat{\psi}_{\beta r}}{n_P \lambda_1 \lambda_4 \hat{\psi}_r^2}\left(-\dot{\hat{\omega}}_r - \lambda_4 \tau_L - \lambda_4 B \hat{\omega}_r\right) \tag{29}$$

$$i_{\beta sref} = \frac{\hat{\psi}_{\beta r}}{\lambda_3}\left(\frac{\dot{\hat{\psi}}_r}{\hat{\psi}_r} + \lambda_2\right) + \frac{\hat{\psi}_{\alpha r}}{n_P \lambda_1 \lambda_4 \hat{\psi}_r^2}\left(\dot{\hat{\omega}}_r + \lambda_4 \tau_L + \lambda_4 B \hat{\omega}_r\right) \tag{30}$$

where $\lambda_1 = \frac{n_P L_m}{J L_r}$, $\lambda_2 = \frac{R_r}{L_r}$, $\lambda_3 = \frac{L_m R_r}{L_r}$, $\lambda_4 = \frac{1}{J}$, $\dot{\hat{\omega}}_r$ is given by differentiating (18) and $\dot{\hat{\psi}}_r$ is given by:

$$-\lambda_2 \hat{\psi}_r + \lambda_3 \frac{\hat{\psi}_{\alpha r} i_{\alpha s} + \hat{\psi}_{\beta r} i_{\beta s}}{\hat{\psi}_r} \tag{31}$$

If ω_{r-ref} and ψ_{r-ref} represents the reference speed and flux respectively, the speed and flux tracking errors are $e_{\omega_r} = \omega_{r-ref} - \hat{\omega}_r$ and $e_{\psi_r} = \psi_{r-ref} - \hat{\psi}_r$ respectively. $\dot{\hat{\omega}}_r$ and $\dot{\hat{\psi}}_r$ in (29) and (30) formulate these tracking errors.

VI. Comparison with Conventional and HOSMC based FOC

In order to validate the robustness and efficacy of the proposed LPV based control scheme, it is compared with the sensorless conventional FOC as explained in Section III-B and also with a higher order sliding mode control (HOSMC) based FOC technique presented in [15] at a higher temperature. For exact comparison, the IM parameters originally given in [15]

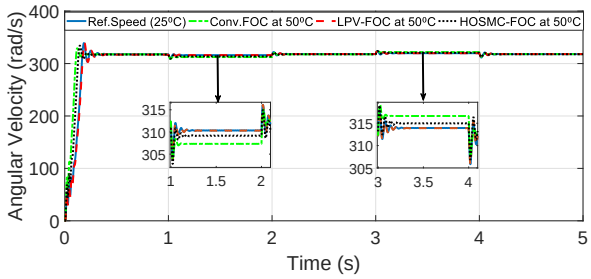

Fig. 4: Thermally degraded speed of IM with and without LPV

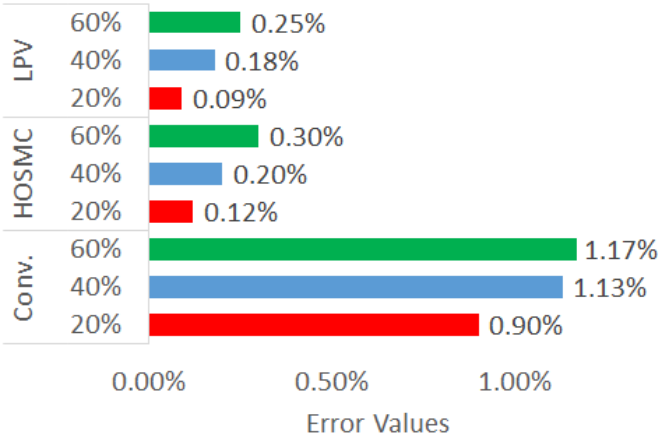

Fig. 5: Performance comparison for stator resistance variations

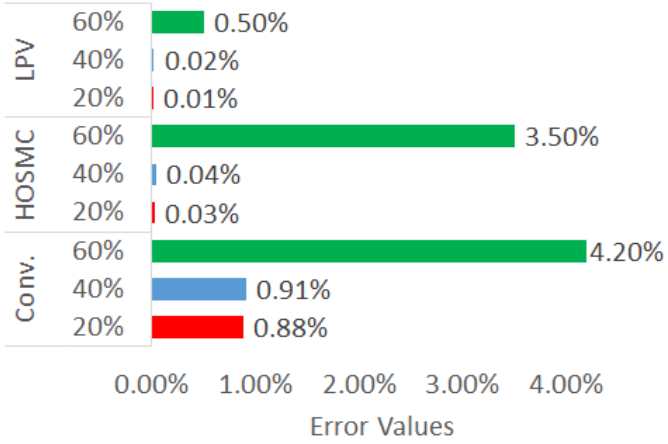

Fig. 6: Performance comparison for rotor resistance variations

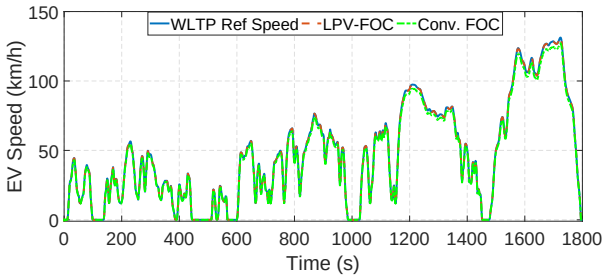

Fig. 8: WLTP Class 3 based EV speed tracking with and without LPV at 50°C

are used i.e. L_s = 400mH, L_r = 412.8mH, R_s = 14.1Ω, R_r = 10.1Ω, L_m = 377mH and J = 0.01 kg.m^2. The same speed reference profile is used as in Section III-B and the comparison of the mentioned control techniques is shown in Fig. 4. It is quite clear from the comparison that LPV-FOC estimates and tracks the speed more accurately than its control counterparts even at higher temperatures. The percentage errors in tracking the angular velocity for stator and rotor resistance variations are compared in Figs. 5 and 6 respectively. The changes in the nominal values of resistances are considered for 20-60% as given in [15]. The negative sign with the error values is ignored just for the ease in visualization of bar charts. It can be seen from the comparison of percentage errors that LPV based FOC performs better than conventional and HOSMC based FOC in the presence of significant variations in machine resistances.

VII. LPV-IM BASED EV PERFORMANCE VALIDATION

As a common trend in the automotive community for the performance validation of control techniques [27], a MATLAB-based EV model simulator is developed and tested against the WLTP Class 3 at 50°C to validate the robust performance of the proposed LPV controller based FOC. The simulator is also capable of performing IM evaluation using conventional FOC. The rated values of the vehicle parameters are: mass (m) = 1000kg, tire radius (R_{tire}) = 0.2m, frontal area (A_f) = 2.1m^2, coefficient of rolling resistance (C_r) = 0.014 and coefficient of aerodynamic drag (C_d) = 0.4m. The complete EV control architecture is shown in Fig. 7. The driver in the figure is inherently a proportional-integral (PI) controller that gets the WLTP Class 3 speed as a reference and generates the driving command in the form of an electromagnetic torque. This command is given to the LPV controller block which acts as the main control of electrified powertrain of EV. The control signal generated in the form of voltage flows from the LPV controller block to the IM, which is also receiving DC battery power through an inverter. Transmission is between the IM and EV dynamics. Finally, the EV speed is fed back to the driver block.

In order to validate the efficacy of the proposed LPV controller-observer set, a temperature profile generated from a model based estimation of stator and rotor resistance is considered throughout the WLTP Class 3 driving cycle, which consists of acceleration, deceleration and constant speed. These resistances are given by [32], [33]:

$$R_r = \sqrt{\omega_{sl}^2 L_r \left[\frac{\omega_e L_m^2}{\frac{Q}{I_s^2} + \omega_e L_s} - L_r \right]} \tag{32}$$

$$R_s = kR_r \tag{33}$$

where ω_{sl} and ω_e are the slip and electrical frequency respectively. The tracking of the desired vehicle speed for conventional and LPV controller based FOC is shown in Fig. 8 which verifies the robust performance of LPV over conventional FOC even at a higher temperature. The IM flux extracted through the LPV observer is shown in Fig. 9.

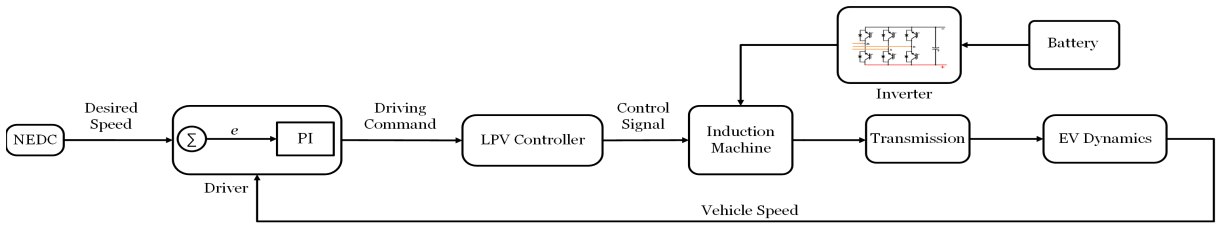

Fig. 7: Electric vehicle control system architecture

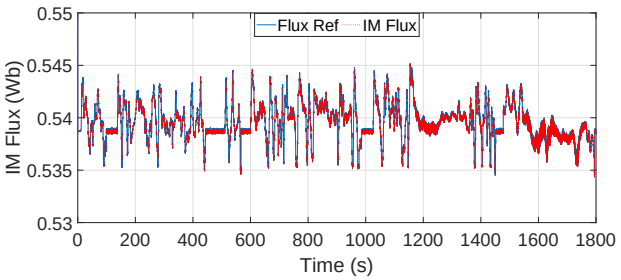

Fig. 9: Induction machine flux w.r.t WLTP Class 3 speed reference

Fig. 10: Induction machine based electrical drive setup

VIII. Experimental Validation

The simulation results obtained in the previous section are validated on an IM drive hardware setup as shown in Fig. 10 to verify that the proposed LPV controller-observer set fully addresses the speed degradation issue due to the IM parameter (stator and rotor resistance) variations caused by the change in temperature. The setup mainly consists of an autotransformer, an inverter for motor control, a 2.2 kW induction motor and an NI myRIO 1900 based controller kit. The controller programming algorithm is implemented in this kit which is interfaced with a PC. The data communication, downloading and data logging functions are performed by the microprocessor. A DL 1019P (magnetic powder brake) is used in conjunction with a DL 2006E (load cell) with a range of 150N. A DL 2031M (optical transducer) is used for rotating speed measurement through an encoder disc based slotted optical switch. This section is further classified into three sub sections based on the experiments performed.

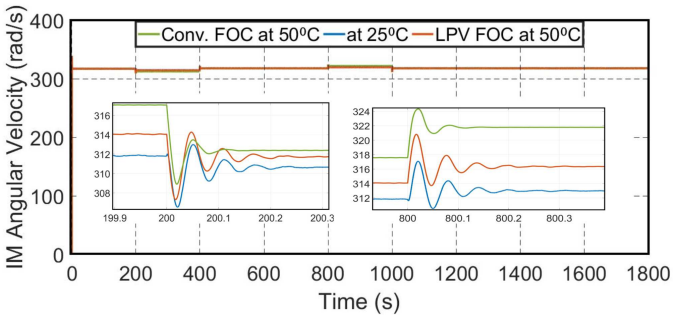

Fig. 11: Experimental result: thermal degradation of IM speed with and without LPV

A. Degradation in IM Speed

In EV based applications, repeated starts and stops along with large inertial loads increase the temperature of traction (induction) machine which results in its mechanical speed's degradation. This effect is shown in Fig. 11 by measuring the IM speed with conventional FOC at nominal (25°C) and increased (50°C) temperatures for a relatively longer period of time. IM speed obtained through LPV controller based FOC at 50°C is also shown. The zoomed plots at transitions clearly validate the improved speed performance with LPV controller. Even at an increased (50°C) temperature, LPV controller keeps the speed performance quite close to the nominal conditions. Moreover, the short time based, closeup view of stator voltages and currents measured at 50°C in case of LPV-FOC and conventional FOC are also presented in Figs. 12 and 13. It can be observed from the voltage and current waveforms that at an elevated drive temperature, the voltage and current demands in case of conventional FOC increases significantly in comparison with LPV-FOC which ultimately causes excessive supply (battery) utilization resulting in performance degradation of IM drive. The effect of load torque can also be seen in the voltage and current waveforms.

B. WLTP Class 3 Analysis for Speed Degradation

In this experiment, WLTP Class 3 based speed is provided as a reference to the controlled IM electrical drive at an elevated temperature (50°C). It can be observed from Fig. 14 that, even during rapid starts and stops, elevated temperatures and large inertial loads, the LPV controller based FOC provides excellent mechanical speed tracking as compared to the conventional FOC. Comparison of the error values of WLTP Class 3 speed tracking with conventional and LPV controller

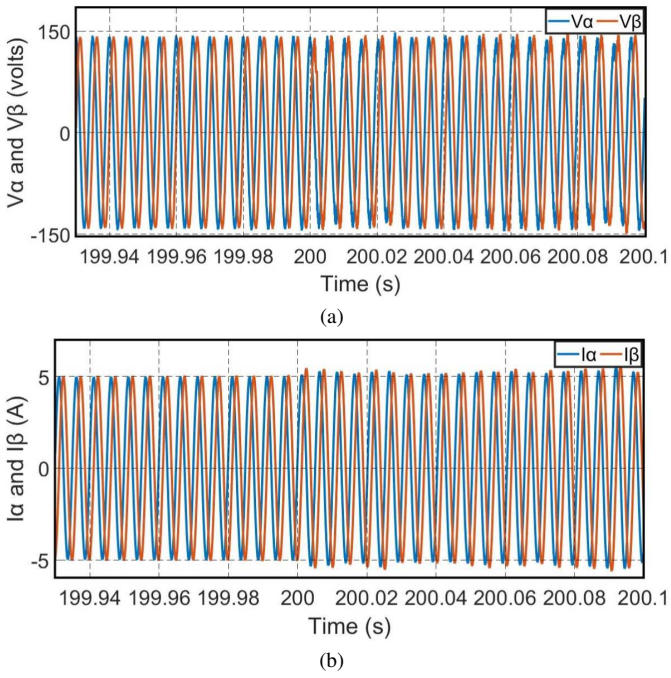

Fig. 12: LPV-FOC at 50°C: (a) Voltages (b) Currents

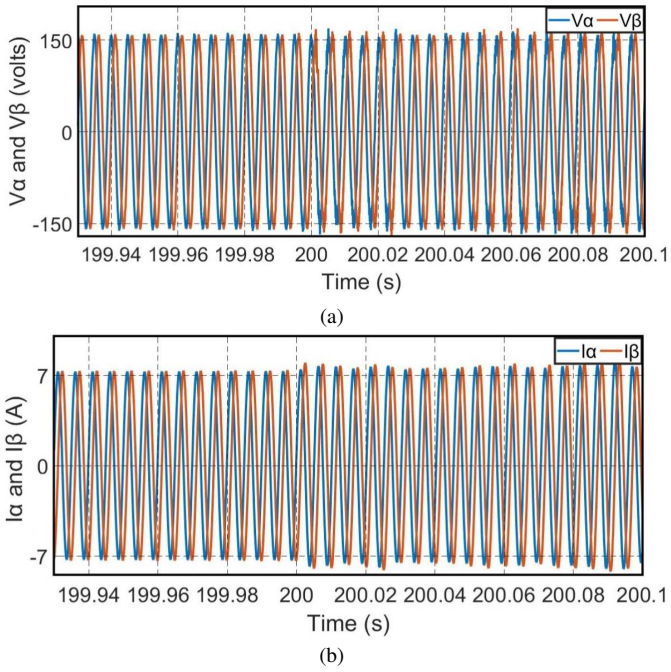

Fig. 13: Conventional FOC at 50°C: (a) Voltages (b) Currents

based FOC obtained through simulation and experimental results is given in Table III. The closeup view for the short time interval of stator voltages and currents measured at 50°C in case of conventional FOC and LPV-FOC are also presented in Figs. 15 and 16. It can be inferred from voltage and current waveforms that at an increased drive temperature, the voltage and current demands in case of conventional FOC are greater than that of LPV-FOC which ultimately causes excessive supply (battery) utilization to deliver the necessary torque resulting in performance degradation of IM drive.The efficacy

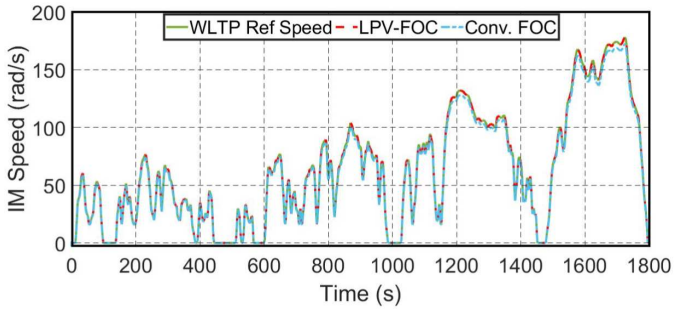

Fig. 14: Experimental result: WLTP Class 3 speed tracking of IM with and without LPV at 50°C

TABLE III: Comparison of WLTP Class 3 Based Speed Tracking

Error	Simulation		Experiment	
	Conv. FOC	LPV-FOC	Conv. FOC	LPV-FOC
RMSE	0.2328	0.0938	0.2457	0.1133

and robust performance of the proposed LPV controller-observer set can be concluded from these comparisons.

C. Sliding Mode Controller-Observer Set Comparison

A first-order Sliding Mode Control (SMC) technique is presented in [12] to obviate the control, flux and speed estimation of induction machine. The LPV control technique proposed in this paper is compared with the SMC by generating similar speed profile and stator resistance variation as presented in [12]. The speed and current tracking for both control techniques are compared in Figs. 17 and 18. The proposed controller accuracy is assessed quantitatively to be 99.2% in comparison with 98% from the speed tracking results. Moreover, the considered variations in stator and rotor

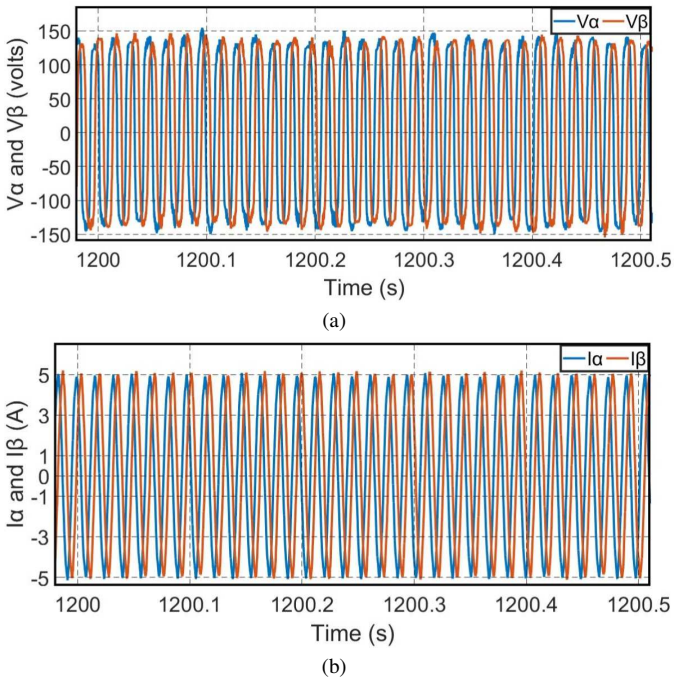

Fig. 15: LPV-FOC at 50°C: (a) Voltages (b) Currents

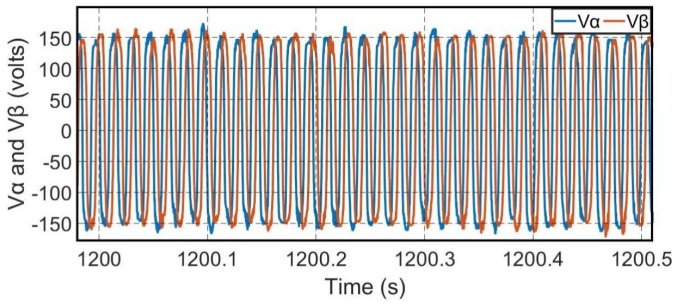

(a)

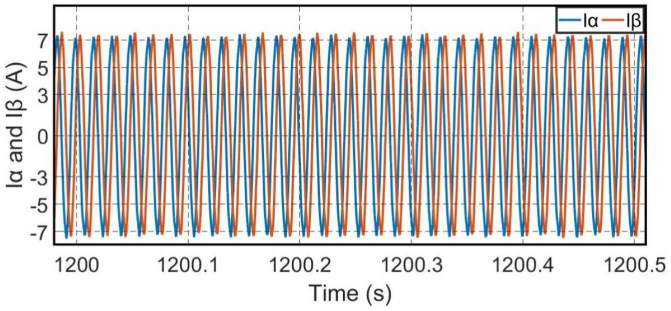

(b)

Fig. 16: Conventional FOC at 50°C: (a) Voltages (b) Currents

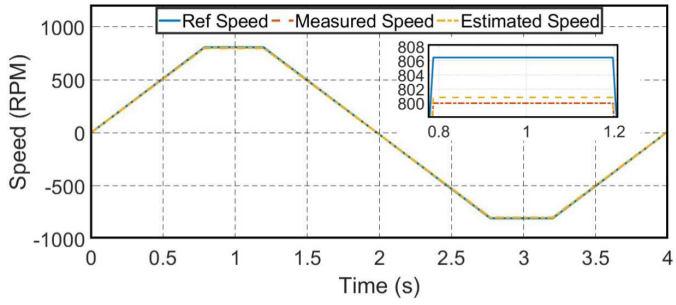

(a)

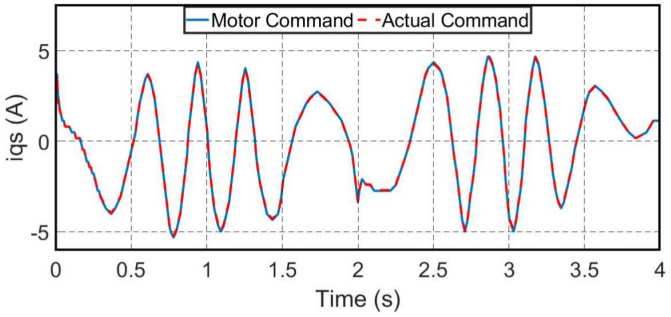

(b)

Fig. 17: LPV-FOC (a) Speed tracking (b) Current tracking

resistance are larger than those in [12]. Hence, LPV provides a better robust control stability and more accurate estimation even with the varying machine parameters.

IX. Conclusion

This paper presents an LPV control technique in FOC frame to improve the speed performance of an IM based electric vehicle by catering the thermal degradation in its mechanical speed in the presence of varying TMD parameters (stator and

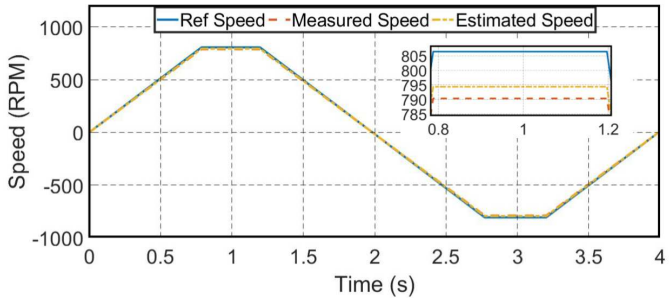

(a)

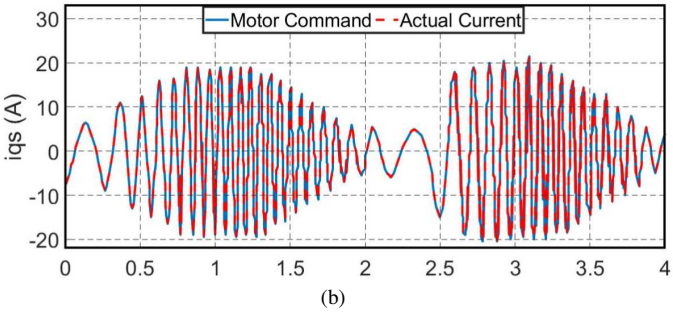

(b)

Fig. 18: Conventional FOC (a) Speed tracking (b) Current tracking

rotor resistance). The estimation of the thermally degraded flux and speed are addressed by a robust LPV observer. A linear matrix inequalities based output feedback LPV robust controller is designed and implemented on an electrical drive setup. A comparison of the proposed LPV controller based FOC with its control counterparts i.e. conventional FOC, SMC and HOSMC is also presented that affirms its effectiveness and advantages. Nonlinear MATLAB-based simulations as well as experimental results are presented that validates the robustness of the proposed control technique, tested against the WLTP Class 3 at various temperature conditions. In future, the control of thermal effects for a permanent magnet machine will be addressed in the LPV environment.

Appendix

The LPV controller gains at vertex 2 are given as:

$$A_K(2) = 1 \times 10^7$$

$$\begin{bmatrix} -0.0000 & 0.0000 & -0.0000 & 0.0000 & -0.0019 & -0.0071 \\ -0.0000 & -0.0000 & -0.0000 & -0.0000 & 0.0071 & -0.0019 \\ 0.0008 & -0.0002 & -0.0042 & 0.0000 & 1.4086 & -0.4047 \\ 0.0002 & 0.0008 & -0.0000 & -0.0042 & 0.4047 & 1.4086 \\ -0.0000 & -0.0000 & 0.0001 & 0.0000 & -0.0268 & -0.0000 \\ 0.0000 & -0.0000 & -0.0000 & 0.0001 & 0.0000 & -0.0268 \end{bmatrix}$$

$$B_K(2) = \begin{bmatrix} 0.0009 & 0.2690 \\ 0.2690 & -0.0009 \\ 0.1916 & -0.8954 \\ -0.8954 & -0.1916 \\ 14.8308 & 222.6213 \\ 222.6213 & -14.8308 \end{bmatrix}, D_K(2) = \begin{bmatrix} 0 & 0 \\ 0 & 0 \end{bmatrix}$$

$$C_K(2) = 1 \times 10^5$$

$$\begin{bmatrix} 0.0003 & -0.0012 & 0.0006 & -0.0028 & 0.0673 & 1.0112 \\ -0.0012 & -0.0003 & -0.0028 & -0.0006 & 1.0112 & -0.0673 \end{bmatrix}$$

The LPV observer gains for vertices 1 and 2 are given as:

$$L_1 = \begin{bmatrix} 39.5 & 0 \\ 0 & 39.5 \\ 6 & 60.3 \\ -60.3 & 6 \end{bmatrix}, L_2 = \begin{bmatrix} 43.8 & 0 \\ 0 & 43.8 \\ 8 & -61.5 \\ 61.5 & 8 \end{bmatrix}$$

ACKNOWLEDGMENT

The authors are grateful to the Electrical Drives Lab, University of Engineering & Technology, Lahore for providing tremendous support in the experimental facilities.

REFERENCES

[1] X. Zhao and S. Niu, "Design and optimization of a novel slot-pm-assisted variable flux reluctance generator for hybrid electric vehicles," *IEEE Transactions on Energy Conversion*, vol. 33, no. 4, pp. 2102–2111, 2018.

[2] T. D. Do, H. H. Choi, and J.-W. Jung, "Nonlinear optimal dtc design and stability analysis for interior permanent magnet synchronous motor drives," *IEEE/ASME Transactions on Mechatronics*, vol. 20, no. 6, pp. 2716–2725, 2015.

[3] A. Haddoun, M. Benbouzid, D. Diallo, R. Abdessemed, J. Ghouili, and K. Srairi, "Modeling, analysis, and neural network control of an ev electrical differential," *IEEE Transactions on Industrial Electronics*, vol. 55, no. 6, pp. 2286–2294, 2008.

[4] J. De Santiago, H. Bernhoff, B. Ekergård, S. Eriksson, S. Ferhatovic, R. Waters, and M. Leijon, "Electrical motor drivelines in commercial all-electric vehicles: A review," *IEEE Transactions on Vehicular Technology*, vol. 61, no. 2, pp. 475–484, 2012.

[5] J. Yu, W. Pei, and C. Zhang, "A loss-minimization port-controlled hamilton scheme of induction motor for electric vehicles," *IEEE/ASME Transactions on Mechatronics*, vol. 20, no. 6, pp. 2645–2653, 2015.

[6] S. Yang, D. Ding, X. Li, Z. Xie, X. Zhang, and L. Chang, "A novel online parameter estimation method for indirect field oriented induction motor drives," *IEEE Transactions on Energy Conversion*, vol. 32, no. 4, pp. 1562–1573, 2017.

[7] J. L. Gonzalez-Cordoba, R. A. Osornio-Rios, D. Granados-Lieberman, R. d. J. Romero-Troncoso, and M. Valtierra-Rodriguez, "Thermal-impact-based protection of induction motors under voltage unbalance conditions," *IEEE Transactions on Energy Conversion*, vol. 33, no. 4, pp. 1748–1756, 2018.

[8] E. M. Adzic, M. S. Adzic, V. A. Katic, D. P. Marcetic, and N. L. Celanovic, "Development of high-reliability ev and hev im propulsion drive with ultra-low latency hil environment," *IEEE Transactions on Industrial Informatics*, vol. 9, no. 2, pp. 630–639, 2013.

[9] S. Dilmi and S. Yurkovich, "Nonlinear torque control of the induction motor in hybrid electric vehicle applications," in *Proceedings of the 2005, American Control Conference, 2005.* IEEE, 2005, pp. 3001–3006.

[10] B. Tabbache, M. E. H. Benbouzid, A. Kheloui, and J.-M. Bourgeot, "Virtual-sensor-based maximum-likelihood voting approach for fault-tolerant control of electric vehicle powertrains," *IEEE Transactions on Vehicular Technology*, vol. 62, no. 3, pp. 1075–1083, 2013.

[11] R. Marino, S. Scalzi, P. Tomei, and C. Verrelli, "Fault-tolerant cruise control of electric vehicles with induction motors," *Control Engineering Practice*, vol. 21, no. 6, pp. 860–869, 2013.

[12] H.-u. Rehman, "Elimination of the stator resistance sensitivity and voltage sensor requirement problems for dfo control of an induction machine," *IEEE Transactions on Industrial Electronics*, vol. 52, no. 1, pp. 263–269, 2005.

[13] J. Guzinski and H. Abu-Rub, "Sensorless induction motor drive for electric vehicle application," *International Journal of Engineering, Science and Technology*, vol. 2, no. 10, pp. 20–34, 2010.

[14] R. De Castro, R. E. Araújo, and D. Freitas, "Wheel slip control of evs based on sliding mode technique with conditional integrators," *IEEE Transactions on Industrial Electronics*, vol. 60, no. 8, pp. 3256–3271, 2013.

[15] J. R. Dominguez, C. Mora-Soto, S. Ortega-Cisneros, J. J. R. Panduro, and A. G. Loukianov, "Copper and core loss minimization for induction motors using high-order sliding-mode control," *IEEE transactions on Industrial Electronics*, vol. 59, no. 7, pp. 2877–2889, 2012.

[16] B. Beltran, M. E. H. Benbouzid, and T. Ahmed-Ali, "Second-order sliding mode control of a doubly fed induction generator driven wind turbine," *IEEE Transactions on Energy Conversion*, vol. 27, no. 2, pp. 261–269, 2012.

[17] L. Zhao, J. Huang, H. Liu, B. Li, and W. Kong, "Second-order sliding-mode observer with online parameter identification for sensorless induction motor drives," *IEEE Transactions on Industrial Electronics*, vol. 61, no. 10, pp. 5280–5289, 2014.

[18] P. Apkarian, "Lmi techniqes in control engineering from theory to practice," in *IEEE CDC'96 Workshop*, 1996.

[19] E. Prempain, I. Postlethwaite, and A. Benchaib, "A linear parameter variant h∞ control design for an induction motor," *Control Engineering Practice*, vol. 10, no. 6, pp. 633–644, 2002.

[20] K. Dalila, M. Abdessalem, D. Said, and L. Chrifi-Alaoui, "Robust linear parameter varying induction motor control with polytopic models," *Serbian Journal of Electrical Engineering*, vol. 10, no. 2, pp. 335–348, 2013.

[21] A. Salem, A. S. Tlili, and N. B. Braiek, "On the polytopic and multimodel state observers of induction motors," *Journal of Automation and Systems Engineering (JASE)*, vol. 2, no. 4, pp. 235–247, 2008.

[22] K. Zhou, J. C. Doyle, K. Glover *et al.*, *Robust and optimal control*. Prentice Hall New Jersey, 1996, vol. 40.

[23] F. Farhani, C. B. Regaya, A. Zaafouri, and A. Chaari, "A quasi linear parameter varying approach to robust control of an induction machine," in *Systems, Signals & Devices (SSD), 2013 10th International Multi-Conference on*. IEEE, 2013, pp. 1–5.

[24] F. Blanchini, D. Casagrande, S. Miani, and U. Viaro, "An lpv control scheme for induction motors," in *Decision and Control (CDC), 2012 IEEE 51st Annual Conference on*. IEEE, 2012, pp. 7602–7607.

[25] D. K. Abdessalem, D. Said *et al.*, "Linear parameter varying induction motor control with two-degree-of freedom controller," in *Power Engineering, Energy and Electrical Drives (POWERENG), 2013 Fourth International Conference on*. IEEE, 2013, pp. 1748–1752.

[26] S. N. Ali, A. Hanif, M. Hossain, and V. Sharma, "An lpv h∞ control design for the varying rotor resistance effects on the dynamic performance of induction motors," in *2018 IEEE 27th International Symposium on Industrial Electronics (ISIE)*. IEEE, 2018, pp. 114–119.

[27] Z. Yang, F. Shang, I. P. Brown, and M. Krishnamurthy, "Comparative study of interior permanent magnet, induction, and switched reluctance motor drives for ev and hev applications," *IEEE Transactions on Transportation Electrification*, vol. 1, no. 3, pp. 245–254, 2015.

[28] A. Hanif, S. N. Ali, Q. Ahmed, A. Bhatti, G. Yin, and M. H. Jaffery, "Effect of variation in rotor resistance on the dynamic performance of induction motor," in *Control Conference (CCC), 2016 35th Chinese*. IEEE, 2016, pp. 9524–9529.

[29] M. A. Valenzuela, J. Tapia, and J. A. Rooks, "Thermal evaluation of tefc induction motors operating on frequency controlled variable speed drives," in *Conference Record of the 2003 Annual Pulp and Paper Industry Technical Conference, 2003.* IEEE, 2003, pp. 164–170.

[30] S. N. Ali, A. Hanif, and Q. Ahmed, "Review in thermal effects on the performance of electric motors," in *Intelligent Systems Engineering (ICISE), 2016 International Conference on*. IEEE, 2016, pp. 83–88.

[31] H. Werner, "Optimal and robust control-lecture notes," *Technical University Hamburg-Harburg, Institute of Control Engineering*, 2004.

[32] P. Zhang, Y. Du, T. G. Habetler, and B. Lu, "A survey of condition monitoring and protection methods for medium-voltage induction motors," *IEEE Transactions on Industry Applications*, vol. 47, no. 1, pp. 34–46, 2011.

[33] R. Beguenane and M. E. H. Benbouzid, "Induction motors thermal monitoring by means of rotor resistance identification," *IEEE Transactions on Energy Conversion*, vol. 14, no. 3, pp. 566–570, 1999.